Bioactive Materials 18 (2022) 539–551

Contents lists available at ScienceDirect

Bioactive Materials

journal homepage: www.keaipublishing.com/en/journals/bioactive-materials

# Free or fixed state of nHAP differentially regulates hBMSC morphology and osteogenesis through the valve role of ITGA7

Fangyuan Bao [a,c,1], Junzhi Yi [a,c,1], Yixiao Liu [a,c,1], Yuliang Zhong [a], Hui Zhang [a], Zhonglin Wu [a,c], Boon Chin Heng [e], Ying Wang [a,c], Ziyang Wang [c], Lizi Xiao [f], Hua Liu [a,c,d], Hongwei Ouyang [a,b,c,d,**], Jing Zhou [a,c,d,*]

[a] Dr Li Dak Sum & Yip Yio Chin Center for Stem Cells and Regenerative Medicine, and Department of Orthopedic Surgery of The Second Affiliated Hospital, Zhejiang University School of Medicine, Hangzhou, PR China
[b] Department of Sports Medicine, Zhejiang University School of Medicine, Hangzhou, PR China
[c] Zhejiang University-University of Edinburgh Institute, Zhejiang University School of Medicine, and Key Laboratory of Tissue Engineering and Regenerative Medicine of Zhejiang Province, Zhejiang University School of Medicine, Hangzhou, PR China
[d] China Orthopedic Regenerative Medicine Group (CORMed), Hangzhou, PR China
[e] School of Stomatology, Peking University, Beijing, PR China
[f] Zhongshan School of Medicine, Sun Yat-sen University, Guangzhou, PR China

ARTICLE INFO

*Keywords:*
Applied forms
nHAP
Osteogenesis
ITGA7

ABSTRACT

Nano-hydroxyapatite (nHAP) has been widely used in bone repair as an osteo-inductive and naturally-occurring material. However, the optimal applied form of nHAP and the underlying mechanisms involved remain unclear. Herein, to investigate into these, a range of corresponding models were designed, including three applied forms of nHAP (Free, Coating and 3D) that belong to two states (Free or fixed). The results indicate that when fixed nHAP was applied in the 3D form, optimal osteogenesis was induced in human bone marrow stem cells (hBMSCs) with increased bone volume via integrin α7 (ITGA7)-mediated upregulation of the PI3K-AKT signaling pathway, while contrary results were observed with free nHAP. Ectopic osteogenesis experiments in mice subcutaneous transplantation model further confirmed the different tendencies of ITGA7 expression and osteogenesis of hBMSCs in free and fixed states of nHAP. Our results revealed that the two states of nHAP play a different regulatory role in cell morphology and osteogenesis through the valve role of ITGA7, providing cues for better application of nanoparticles and a potential new molecular target in bone tissue engineering.

## 1. Introduction

Nanohydroxyapatite (nHAP) is a type of promising nanoparticles in bone tissue engineering, as one of the major inorganic components assembled with collagen to synthesize bone tissues [1]. As a scaffold material, nHAP is similar to native bone architecture in terms of mechanical properties and structures. Thereby providing a microenvironment for osteogenic cells which is conducive to cell proliferation, differentiation and migration, which translates into newly-formed functional bone tissues [2]. In the treatment of bone diseases, applied forms of nHAP mainly can be divided into free state, such as direct injection [3], and fixed state, such as coating on a material [4] and incorporation into 3D scaffolds [39]. And they have both been investigated for promoting bone tissue regeneration. Each applied form of nHAP provides a unique nHAP microenvironment for cells. However, there has so far been a lack of rigorous investigations into which applied form of nHAP can exert optimal effects in specific therapeutic scenarios and which nHAP microenvironmental conformation is optimal for osteogenic differentiation.

Peer review under responsibility of KeAi Communications Co., Ltd.
* Corresponding author. Dr Li Dak Sum & Yip Yio Chin Center for Stem Cells and Regenerative Medicine, and Department of Orthopedic Surgery of The Second Affiliated Hospital, Zhejiang University School of Medicine, Hangzhou, PR China.
** Corresponding author. Dr Li Dak Sum & Yip Yio Chin Center for Stem Cells and Regenerative Medicine, and Department of Orthopedic Surgery of The Second Affiliated Hospital, Zhejiang University School of Medicine, Hangzhou, PR China.
*E-mail addresses:* hwoy@zju.edu.cn (H. Ouyang), zhoujing@zju.edu.cn (J. Zhou).
[1] These authors contributed equally.

https://doi.org/10.1016/j.bioactmat.2022.03.016
Received 12 December 2021; Received in revised form 16 February 2022; Accepted 11 March 2022

As for the underlying mechanisms of the interaction between nanoparticles and cells, many previous studies were based on conventional cell cultures exposed to freely-suspended nanoparticles within culture medium, and then the *in vivo* fixed ones were evaluated to confirm with *in vitro* data [6]. Currently, the incorporation of nHAP into 3D scaffolds are the most extensively applied form, which has so far demonstrated good therapeutic effects in bone tissue engineering [6,7]. However, these studies mainly focused on the repair effects of composite scaffolds, and the regulatory mechanisms of Cell-nHAP interaction are still poorly understood [8]. Some previous studies have tried to explore this mechanism using culture plate seeded with cells and culture medium added with nHAP, even though this is far from being the ideal way to explore *in vivo* mechanism. Therefore, it is imperative to further investigate the underlying regulatory mechanisms of interaction between stem cells and various nHAP microenvironments, especially the 3D one [9].

The integrin family may play a crucial role in this interaction as the major cellular receptors responsible for sensing and manipulating the ECM with integrated topographical and biochemical signals [10]. Kim et al. reported that a nHAP composited material with nano-roughened surface can accelerate the cellular responses through integrin-triggered focal adhesions [11]. The activation of integrin α5 has been shown to play a key role in osteogenesis [12]. And integrin α11 has been reported to be a prerequisite for the maintenance of adult skeletal bone mass [13]. Moreover, the integrin receptors can also mediate the interaction between osteoblasts and HAP substrates [9]. These studies thus suggest that integrins could play a key role in modulating osteogenic differentiation in specific

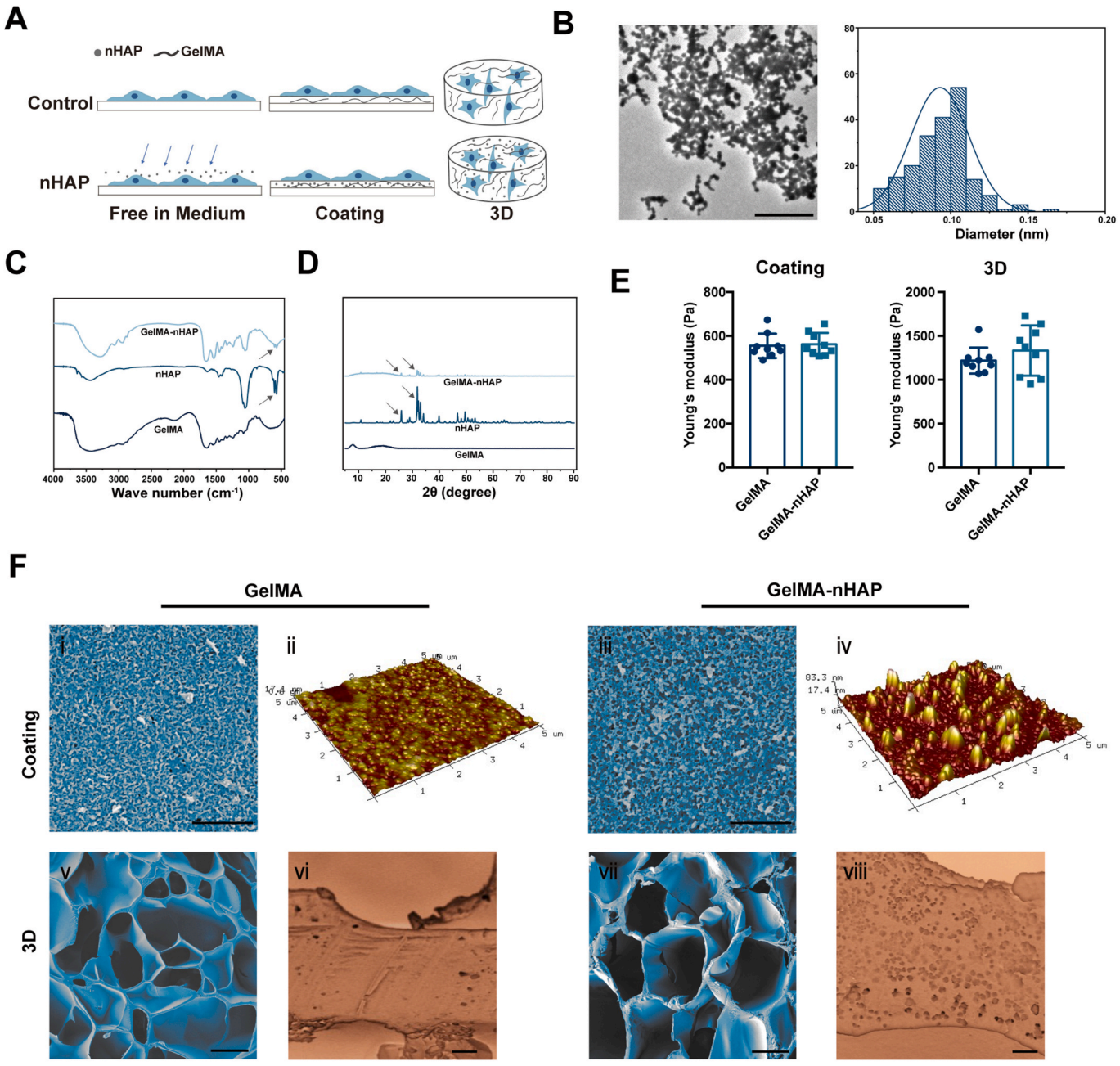


**Fig. 1.** Characterization of different nHAP applied forms. (A) Scheme of three nHAP applied forms with corresponding control group. (B) TEM image of nHAP and the statistical distribution of the sizes is at the right panel. Scale bar = 1 μm (C) FTIR and (D) XRD results of GelMA, nHAP and GelMA-nHAP. (E) Mechanical testing of GelMA and GelMA-nHAP by nanoindenter. (F) SEM images of the morphology of GelMA and GelMA-nHAP in Coating groups (i and iii, scale bar = 500 nm). Atomic Force Microscope (AFM) images of GelMA and GelMA-nHAP (ii and iv). SEM images of 3D scaffolds (v and vii, scale bar = 50 μm) and higher magnification of the cross sections (vi and viii, scale bar = 1 μm).

nHAP microenvironments, though little is known about the specific subunits of the integrin family involved.

In our study, different models of nHAP applied forms, including 3D-nHAP (hydrogel encapsulation), Coating-nHAP (surface coating) and Free-nHAP (free in medium) were established. Each model was paired with a corresponding control group (3D-con, Coating-con and Free-con) with biocompatible GelMA (Gelatin methacryloyl) as a test bed for Coating-nHAP and 3D-nHAP [14]. Our results indicated that increased osteogenesis with marked cell volume expansion in the 3D-nHAP microenvironment, which contrasted with the less-than-optimal and opposite results were observed in the Coating-nHAP and Free-nHAP group, respectively. Furthermore, we elucidated the vital role ITGA7 plays at the early stage of osteogenesis via upregulation of PI3K-AKT signaling pathway. Therefore, these findings reveal the profound effects of different nanoparticle microenvironments on cell morphology and osteogenesis and highlight the critical role of ITGA7 in osteogenic differentiation.

## 2. Results

### 2.1. Characterization of different nHAP applied forms

To obtain a deeper understanding of the models of various nHAP applied forms, we first characterized the morphology as well as physical and chemical properties of nHAP, GelMA and the nanocomposite hydrogels (GelMA-nHAP). The experimental groups designed for systematically investigating the effects of nHAP are illustrated in Fig. 1A and the methods. First, CCK8 analysis and alkaline phosphatase (ALP) staining were performed to determine the concentration of nHAP we would use. The results demonstrated that approximately 100–200 μg/ml nHAP exposed to cell culture medium inhibited cell proliferation and differentiation to the largest degree (Figs. S1A and B, Supporting Information). Combining previous research and ours, we decided to experiment with 167 μg/ml of nHAP to investigate whether it would produce the same effect in other applied forms [15].

To analyze the shape and size distributions of nHAP, we conducted transmission electron microscopy (TEM), and the result revealed a homogeneous particle size distribution with an average diameter of 100 nm (Fig. 1B). To identify the different properties of GelMA, nHAP and GelMA-nHAP, we applied Fourier transform infrared (FTIR) and X-ray diffraction (XRD) (Fig. 1C and D). In the FTIR results, two sharp peaks of nHAP were observed at about 603 $cm^{-1}$ and 564 $cm^{-1}$, which are characteristic of phosphate groups related to nHAP [16], while similar peaks with a lower density were exhibited in GelMA-nHAP and peaks within the different ranges were displayed of GelMA (Fig. 1C). The XRD results revealed the typical intensity peaks of nHAP and the lower intensity peaks of GelMA-nHAP at 25.9° and 31.8° (Fig. 1D), which are attributed to the (002) and (211) planes of the nHAP according to the standard data (JCPDS No. 09-0432) [17]. The alteration of a scaffold may change its mechanical properties [40]. Herein, we measured the Young's modulus of GelMA and GelMA-nHAP in Coating groups and 3D groups, and the results suggested that adding nHAP did not change the mechanical properties of the hydrogels in both Coating and 3D groups at this low concentration of nHAP (Fig. 1E). Therefore, the influence of mechanical properties on cells may be excluded. Next, scanning electron microscopy (SEM) and atomic force microscope (AFM) images revealed that GelMA-nHAP exhibited the increased roughness compared with GelMA both in Coating and 3D groups (Fig. 1F). According to AFM results, the section height of GelMA-nHAP could be up to 100 nm compared with GelMA (Fig. S2A, Supporting Information). Finally , the results of Energy Dispersive Spectroscopy (EDS) showed that GelMA-nHAP had higher ratio of calcium and phosphorus than GelMA (Fig. S2B, Supporting Information).

### 2.2. Biocompatibility of different nHAP microenvironments

First, to investigate the biocompatibility of nHAP in different microenvironments, we evaluated the viability and proliferation of hBMSCs by performing Live/Dead assays and CCK-8 assays. Quantitative analysis of Free groups (Free-con and Free-nHAP) at day 3 and 7 revealed that cell viability was significantly lower in Free-nHAP group than in Free-con group (Fig. S3A, Supporting Information). In Coating groups (Coating-con and Coating-nHAP) and 3D (3D-con and 3D-nHAP) groups, both the nHAP and corresponding control groups exhibited great rate of cell viability (Figs. S3B and C, Supporting Information). Next, cell proliferation analysis by CCK-8 kit on days 1, 3, 5, 7 demonstrated that the proliferation of hBMSCs was inhibited in Free-nHAP microenvironment compared with that in Free-con group, whereas no such difference was observed in Coating groups (Figs. S3D and E, Supporting Information). Interestingly, compared to 3D-con group, nHAP can markedly improve hBMSCs proliferation in a 3D microenvironment (Fig. S3F, Supporting Information). Taken together, our results indicate that fixed nHAP exhibit good biocompatibility, and nHAP plays a differential role in regulating cell proliferation when applied in different forms.

### 2.3. Distinct alteration of cell morphology with different nHAP applied forms

To explore the effects of nHAP on cell morphology via direct cellular response, we seeded cells on the Free, Coating groups and 3D groups. After 72 hours culturing, we found that the cell spreading area and circularity were significantly decreased in the Free-nHAP group (Fig. 2A). Compared to Coating-con group, similar difference in the cell spreading area was also observed in the Coating-nHAP group (Fig. 2B), as shown by fluorescence-labeled phalloidin staining. It should be noted that no significant difference was observed in circularity between the Coating groups. The results of 3D groups revealed that cells exhibited significantly increased cell volume over 3 days within 3D-nHAP microenvironment compared with the 3D-con group, while increased sphericity was not observed (Fig. 2C).

Next, SEM was applied to observe the cell ultrastructure within different nHAP applied forms. The abundance of filopodia contributed to strengthening the adhesive interactions, and thereby sensing the nanoscale biomechanical cues that trigger cellular cascades to regulate cell activity [19]. SEM images indicated that cell membranes were coated by nHAP exposed to the culture medium, and extended less protruded filopodia, which represents the impairment of the cell spreading (Fig. 2D). As soon as nHAP was exposed to physiological fluids, protein corona formed on its surface due to its charge characteristics and high surface area, and then the nHAP would mediate interactions with the cell membrane [20]. In the Coating groups, we observed longer protruded filopodia that was intimately associated with the flatter surface, as compared to Free in Medium groups (Fig. 2E). In the 3D culture, it was difficult to find more detailed information due to the covering of hydrogel, but it was still possible to observe some exposed cells (Fig. 2F). Collectively, our results indicated that different nHAP microenvironments can alter cell size and morphology, as evidenced by the expanded volume in the 3D-nHAP group and reduced cell spreading areas and circularity in the Free-nHAP group, which may be associated with cell differentiation.

### 2.4. Varying trends of hBMSC osteogenic differentiation with different nHAP microenvironments

To evaluate the potential effects of nHAP applied forms on osteogenic differentiation, we analyzed the expression level of osteogenesis-related proteins after 3 and 7 days of culturing hBMSCs in osteogenic-inducing medium with different nHAP microenvironments. First, ALP staining and quantification of ALP expression were performed. In the

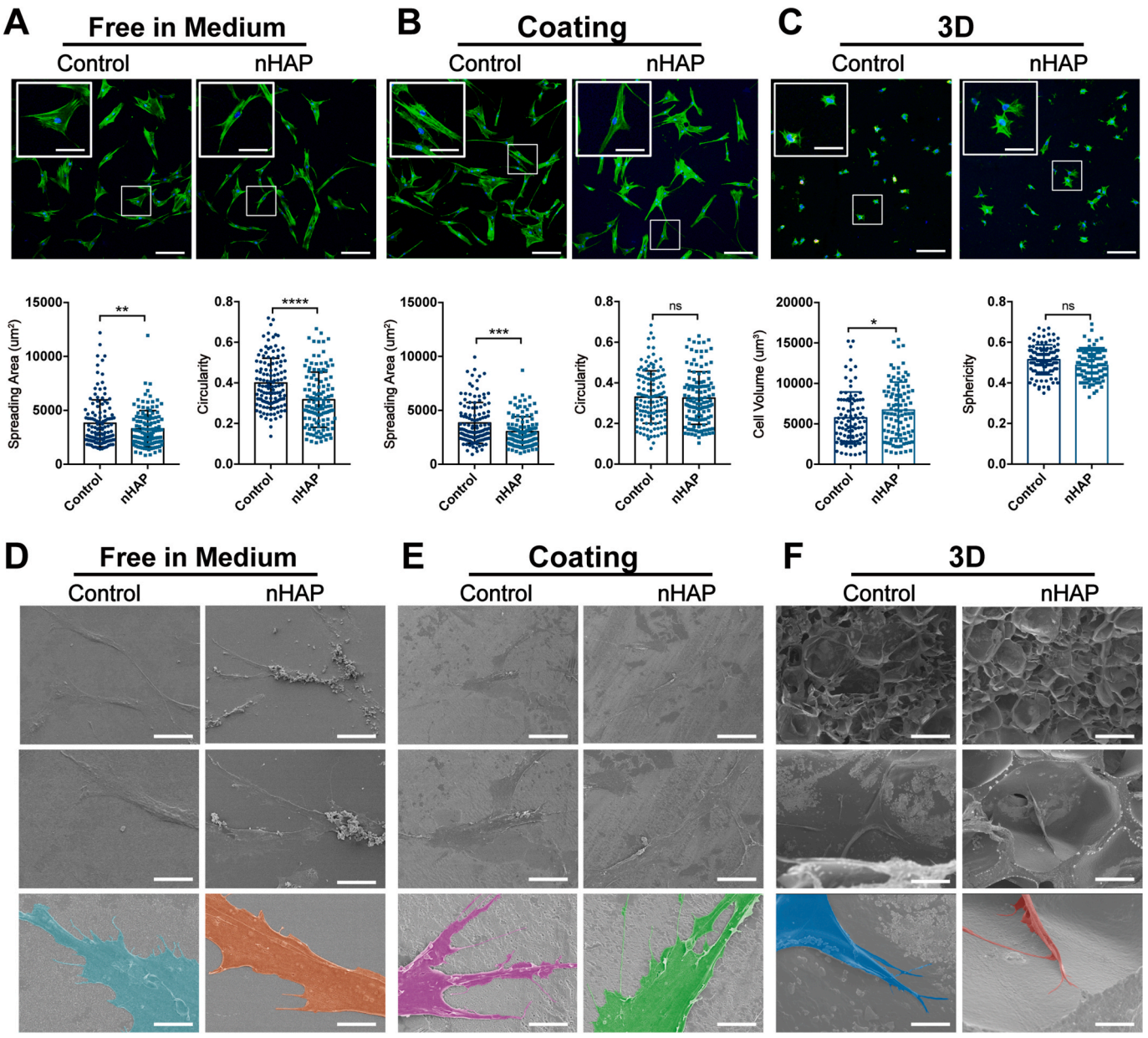


**Fig. 2.** Distinct alteration of cell morphology in different nHAP applied forms. (A), (B) and (C) Representative confocal images and corresponding quantifications (lower panel) of Free (A), Coating (B) and 3D (C) groups. Scale bar = 500 μm, inner scale bar = 200 μm (n = 3, more than 100 single cells were counted); *P < 0.05, **P < 0.01, ***P < 0.001 and ****P < 0.0001. (D), (E) and (F) Surface morphologies of Free (D), Coating (E) and 3D (F) groups under SEM. Scale bars = 50 μm (upper panels), 25 μm (middle panels) and 5 μm (lower panels).

Free in Medium groups, the expression levels of ALP in the Free-nHAP microenvironment were significantly lower than those in the Free-con group at both day 3 and day 7 (Fig. 3A). The gene expression level of *collagen I* (*COL1*) was also remarkably downregulated after 7 days of culturing, thus indicating nHAP-induced impairment of synthesis of extracellular matrix when nHAP was exposed in culture medium (Fig. 3B). In Coating groups, no significant statistical difference in ALP expression was observed after 3 days and 7 days of culturing, whereas the gene expression level of *osteocalcin* (*OCN*) was significantly increased after 7 days of culturing (Fig. 3C and D). The results suggested that the Coating-nHAP microenvironments can enhance osteogenesis, provided that the state of nHAP switched from free suspension to immobilization. Within 3D-nHAP microenvironment, significant increases in ALP staining and quantification were observed at 3 and 7 days after osteoinduction, thus indicating that nHAP could significantly promote hBMSCs osteogenesis in a 3D nHAP microenvironment (Fig. 3E). Interestingly, increased *COL1* expression was displayed in the 3D-nHAP group, which was the opposite compared with that of the Free-nHAP group (Fig. 3F), and the gene expression of *OCN* was also significantly enhanced after 7 days of culturing in 3D-nHAP microenvironment (Fig. 3F).

As an important transcription factor, RUNX2 can promote the expression of osteogenic genes when being translocated into the nuclei of stem cells, exhibited higher nuclear localization in MSCs upon the onset of osteogenesis [21]. The immunofluorescent images of RUNX2 showed that, compared to Free-con group, the Free-nHAP microenvironment inhibited RUNX2 expression, but promoted its nuclear translocation of RUNX2 after 3 days (Fig. 3G), whereas no significant differences were observed in both RUNX2 expression and nuclear translocation in the Coating groups at the same time (Fig. 3H). In 3D-nHAP microenvironments, nHAP was found to significantly promote RUNX2 expression after 3 days, while no significant difference was

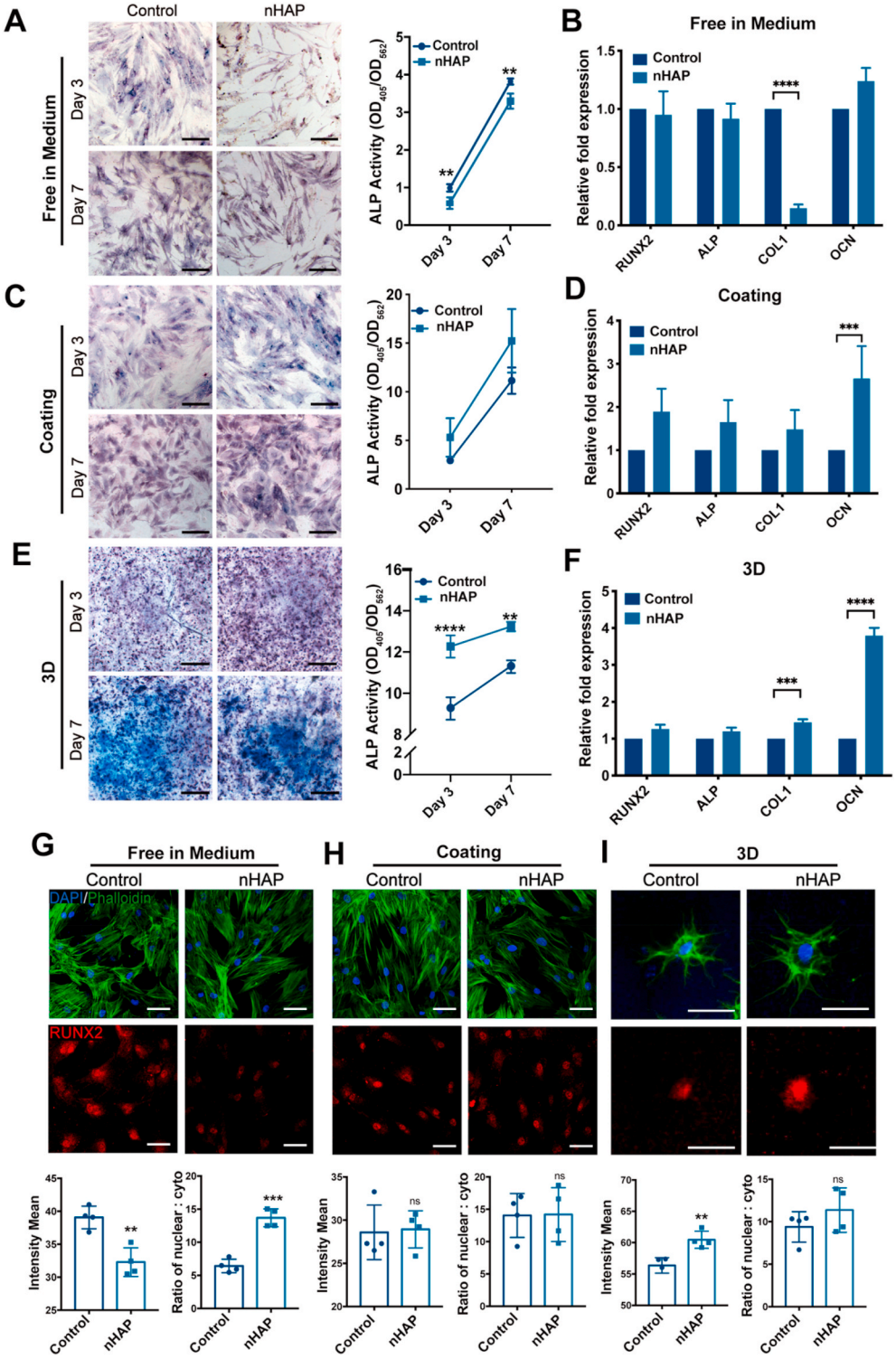


**Fig. 3.** Diverse trends of hBMSC osteogenic differentiation in different nHAP applied forms. (A), (C) and (E) ALP staining of hBMSCs after culturing in osteogenic medium for 3 and 7 days in Free (A), Coating (C) and 3D (E) groups. Corresponding ALP quantifications were located at the right panel. Scale bar = 100 μm for (A) and (C). Scale bar = 500 μm for (E). (B), (D) and (F) Relative mRNA expression levels of osteogenesis-related gene expression at days 7 in Free (B), Coating (D) and 3D (F) groups. (G), (H) and (I) Immunofluorescence staining of RUNX2 and corresponding quantifications in Free (G), Coating (H) and 3D (I) groups. Scale bar = 30 μm for (G) and (H). Scale bar = 20 μm for (I). *p < 0.05, **p < 0.01, ***p < 0.001.

presented in the nuclear translocation between the two groups (Fig. 3I). Taken together, these results presented consistent data, further confirming the correlation between early-stage osteogenesis of hBMSCs and cell spreading areas and volumes. In general, nHAP plays an important role in cell differentiation, and the 3D-nHAP and Coating-nHAP microenvironments exhibited a marked and slight upregulation of osteogenic differentiation, respectively, while the Free-nHAP microenvironments directly impaired osteogenic lineage commitment and ECM expression of hBMSCs.

### 2.5. Transcriptomic analysis of cells cultured with different of nHAP microenvironments

To further clarify the mechanism of how the different nHAP microenvironments influence the osteogenesis, we cultured hBMSCs with nHAP (167 μg/ml) and performed RNA-seq after 7 days to provide a broad overview of early differentiation. Four replicates of hBMSCs in each group were sequenced. First, DEseq2 was conducted to calculate differentially expressed genes (DEGs, q value ≤ 0.05) between nHAP

treated hBMSCs and untreated hBMSCs in each nHAP applied form (Fig. 4A). These results revealed significant changes in hBMSCs gene expression profile with different nHAP microenvironment: in the Free-nHAP microenvironment, 1928 genes were up-regulated and 1919 genes were down-regulated; and in the Coating-nHAP microenvironment, 373 genes were up-regulated and 547 genes were down-regulated; within the 3D-nHAP group, 929 genes were up-regulated and 1227 genes were down-regulated within the 3D-nHAP group (Fig. 4A). Principal component analysis (PCA) was performed to detect the gene-to-gene distances, revealing significant separation of clustering among the expressed genes within different nHAP microenvironments (Fig. 4B). In order to determine the cell fate impacted by nHAP, we analyzed biological processes ($q \leq 0.05$) via gene ontology (GO) enrichment analysis. In the Free-nHAP group, compared to Free-con group, GO terms including cell adhesion (GO:0007155), cell migration (GO:0016477) and angiogenesis (GO:0001525), were significantly down-regulated (Fig. 4C), whereas in the Coating-nHAP group, the same three GO terms were upregulated compared to those of the Coating-con group, thereby indicating that in the Coating-nHAP group osteogenesis was promoted to a certain extent (Fig. 4D). In the 3D nHAP microenvironment, compared to 3D-con, not only were the three GO terms up-regulated, but also osteoblast differentiation (GO:0001649) and skeletal system development (GO:0001501) were induced in the GO up regulation enrichment (Fig. 4E).

To gain further functional insights into the differentially-expressed genes of hBMSCs, ssGSEA (single sample gene set enrichment analysis) analysis was performed and the results revealed normalized enrichment scores (NES) among the different nHAP applied forms. The radar graphs suggested that hBMSCs exhibited the greatest potential for osteogenic differentiation and bone formation within 3D-nHAP microenvironment in terms of bone mineralization, bone maturation, osteoblast differentiation and collagen fibril organization, which was consistent with previous results (Fig. 4F and G). Venn diagram analysis identified the different and similar DEGs (p value $\leq 0.05$) in the three applied forms, and the 573 DEGs were the commonly-expressed genes in all applied forms (Fig. 4H). Next, the Kyoto Encyclopedia of Genes Genomes (KEGG) pathway enrichment analysis was conducted to explore the underlying pathways of the 573 genes and the findings identified focal adhesion, PI3K-AKT signaling pathway and ECM-receptor interaction among the top 10 signaling pathways (Fig. 4I). To further analyze the underlying gene interactions, we depicted the corresponding gene-gene interaction networks(Fig. 4J). Notably, integrin alpha7 (ITGA7) was found to be linked to the before mentioned three pathways, with quite differential expression levels presented among the six groups in the results of heatmap of ITGA (Fig. 4K). The RNA-seq results suggested that the 3D-nHAP microenvironment can further promote hBMSCs osteogenic differentiation than the Coating-nHAP microenvironment, while the Free-nHAP microenvironment inhibited hBMSCs osteogenic differentiation. ITGA7 might thus play an important role in different nHAP applied forms on osteogenesis through PI3K-AKT signaling pathway.

### 2.6. ITGA7 regulates cell morphology and osteogenesis

Based on the RNA-seq analysis, we further confirmed the roles of ITGA7 in the regulation of osteogenic differentiation within the 3D microenvironment. First, the expression of ITGA7 was knocked down using small interference RNA (siRNA). qRT-PCR analysis and ITGA7 staining proved the efficiency of siRNA (Fig. 5A, B and C). Significant down-regulation was observed in the mRNA level of the osteogenic transcription markers (*ALP*, *COL1* and *OCN*), and the protein level of RUNX2 were also significantly down-regulated in the 3D-nHAP group treated with the siRNA after 3 days (Fig. 5A, B and C). Next, the ALP staining and quantification revealed that the ALP expression in 3D-nHAP group was significantly increased compared with 3D-con group at day 3 and day 7, while it was decreased when ITGA7 was inhibited (Fig. 5D and E). Following this, we stained F-actin and analyzed the volume and sphericity of hBMSCs by Imaris software. The results indicated that the knockdown of the expression of ITGA7 could significantly reverse the volume increased by the nHAP and increased the cell sphericity (Fig. 5F and G). The PI3K-AKT pathway has been found to be widely related to osteogenic differentiation [22]. To further explore whether the PI3K-AKT signaling pathway could reciprocally regulate ITGA7, PI3K-AKT signaling was inhibited by MK-2206 2HCl. The qRT-PCR results showed that the expressions of ITGA7 and ALP were suppressed in the 3D-nHAP microenvironment when PI3K-AKT signaling pathway was inhibited (Fig. 5H). The results of western blot demonstrated that PI3K-AKT pathway was down regulated by inhibition of ITGA7 expression, and the down-regulation of PI3K-AKT signaling pathway can also lead to decreased expression of ITGA7 (Fig. 5I). In general, the *in vitro* experiments confirmed that ITGA7 plays a key role in cell morphology during osteogenesis, and that there is a correlation between ITGA7 and PI3K-AKT signaling pathway.

### 2.7. Ectopic osteogenesis of hBMSCs with different nHAP microenvironments in vivo

To further confirm the osteogenic effects of different nHAP microenvironments, ectopic osteogenesis in a mice model was applied. Based on the *in vitro* experiments, the Free in Medium and 3D groups were therefore chosen for further study because of the marked changes and opposite trends. The cell suspensions with Free-nHAP and hBMSC-laden scaffolds with 3D-nHAP *in vivo* were administered into mice by hypodermically injection and subcutaneous implantation of hydrogels into nude mice, respectively (Fig. 6A). After implantation for 2 and 4 weeks, the implants were explanted from the nude mice. Images showed that the implant size of the 4-week groups was much smaller than that of the 2-weeks group, and that some blood vessels were visible in the 3D-nHAP implants (Fig. 6B). The decrease of implant size can be largely attributed to the loss of hBMSCs and the degradation of GelMA. Hematoxylin and eosin (H&E) staining demonstrated that cell lumps were much smaller at 4 weeks compared with the 2-weeks results (Fig. 6C). In addition, the HE results in 3D groups indicated that cells were distributed in a uniformly manner and the secreted matrix was promoted within 3D-nHAP microenvironments because of fewer pores in the hydrogel (Fig. 6C). The immunofluorescent staining of anti-human lamin suggested that hBMSCs could survive up to 4 weeks *in vivo* (Fig. 6D). We observed increased osteogenic differentiation in the 3D-nHAP groups, as indicated by the intensity of RUNX2, OCN and COL1 fluorescence, respectively. The opposite trend was noted in the Free in Medium versus 3D groups in comparison with their corresponding control groups (Fig. 6E and F). In the Free-nHAP group, the protein levels of RUNX2, OCN and COL1 were inhibited compared with those of the Free-con group (Fig. 6E and F). To confirm the role of ITGA7 in osteogenic differentiation, the immunofluorescent staining was performed and the results showed significantly increased ITGA7 expression when cells were encapsulated in 3D-nHAP rather than in the Free-nHAP applied form (Fig. 6G). The quantifications of immunofluorescent were present in Fig. 6H. Collectively, these results suggested that in the 3D-nHAP microenvironments, but not Free-nHAP microenvironments, ITGA7 expression was promoted and osteogenesis enhanced. We thus confirmed the role of ITGA7 and how nHAP affected osteogenesis *in vivo*.

## 3. Discussion

Preliminary studies have been carried out on delivery of nHAP nanoparticles *in situ* via direct injection, coating onto a material or incorporation within a nanocomposite scaffold [3,23,24]. However, inadequate understanding of which applied form of nHAP can exert the optimal effects in specific applications and which relevant nHAP microenvironment is optimal for osteogenic differentiation have thus limited the development of efficacious nano-based therapies. In our study, in order to investigate how various applied forms of nHAP within

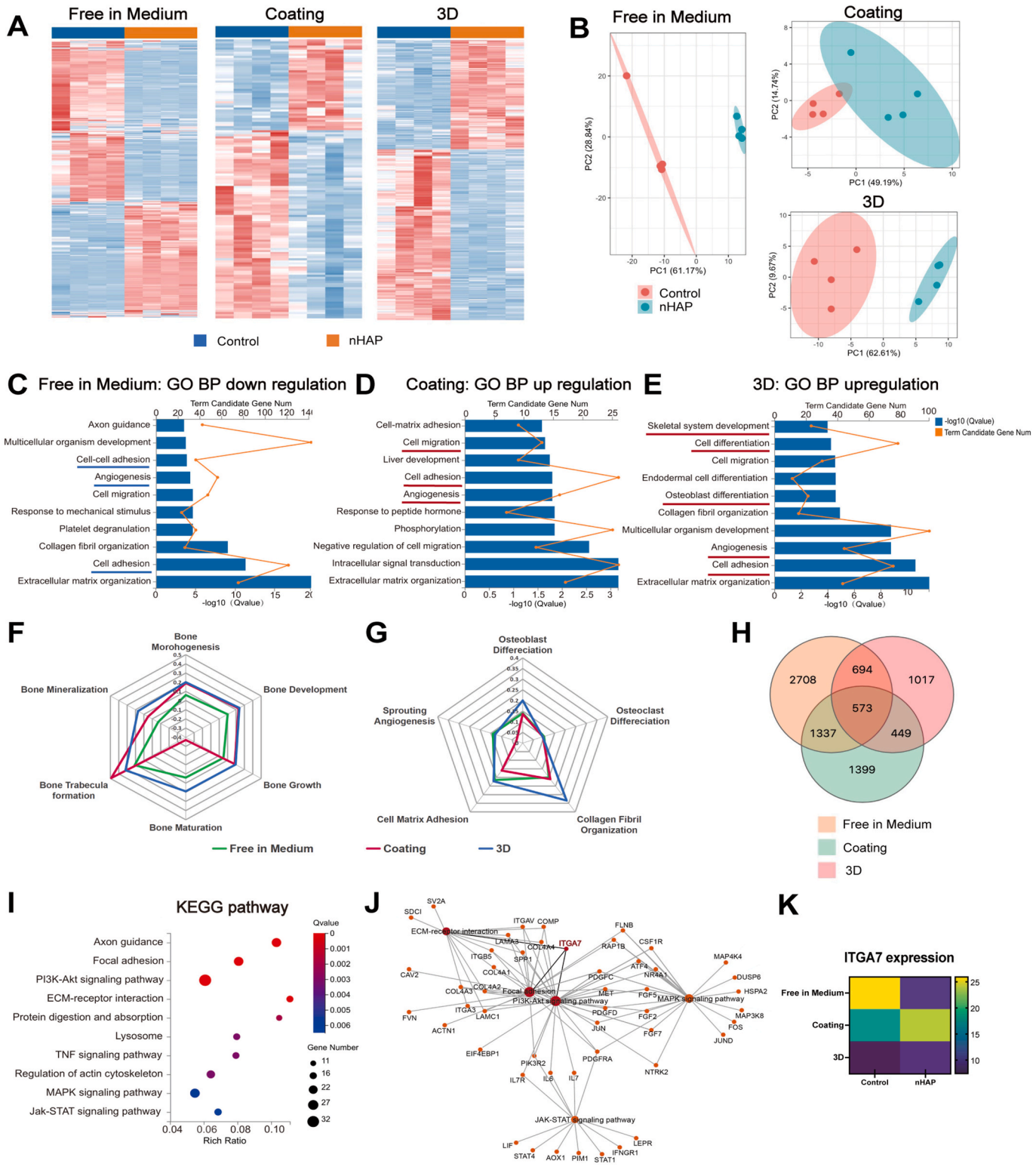


**Fig. 4.** Transcriptomic analysis elucidates different nHAP microenvironments determining cell fate. (A) Heat map of row normalized FPKM z-scores of differentially expressed genes (red: up-regulated, blue: down-regulated) in Free, Coating and 3D groups. (B) Principal component analysis of the gene expression with three nHAP applied forms. (C) Gene ontology (GO) analysis showed down-regulated terms of biological processes in Free-nHAP group compared with corresponding control. (D) and (E) GO analysis showed up-regulated terms of biological processes in Coating (D) and 3D (E) groups compared with corresponding controls. (F) and (G) ssGSEA analysis normalized enrichment score about osteogenesis. (H) Venn diagram indicating the overlap between the DEGs from the comparisons of three applied form of nHAP. (I) Top 10 KEGG pathway and corresponding gene network (J) according to 573 DEGs. (K) The heat map of ITGA7 expression in three different applied forms (yellow: high expression, purple: low expression).

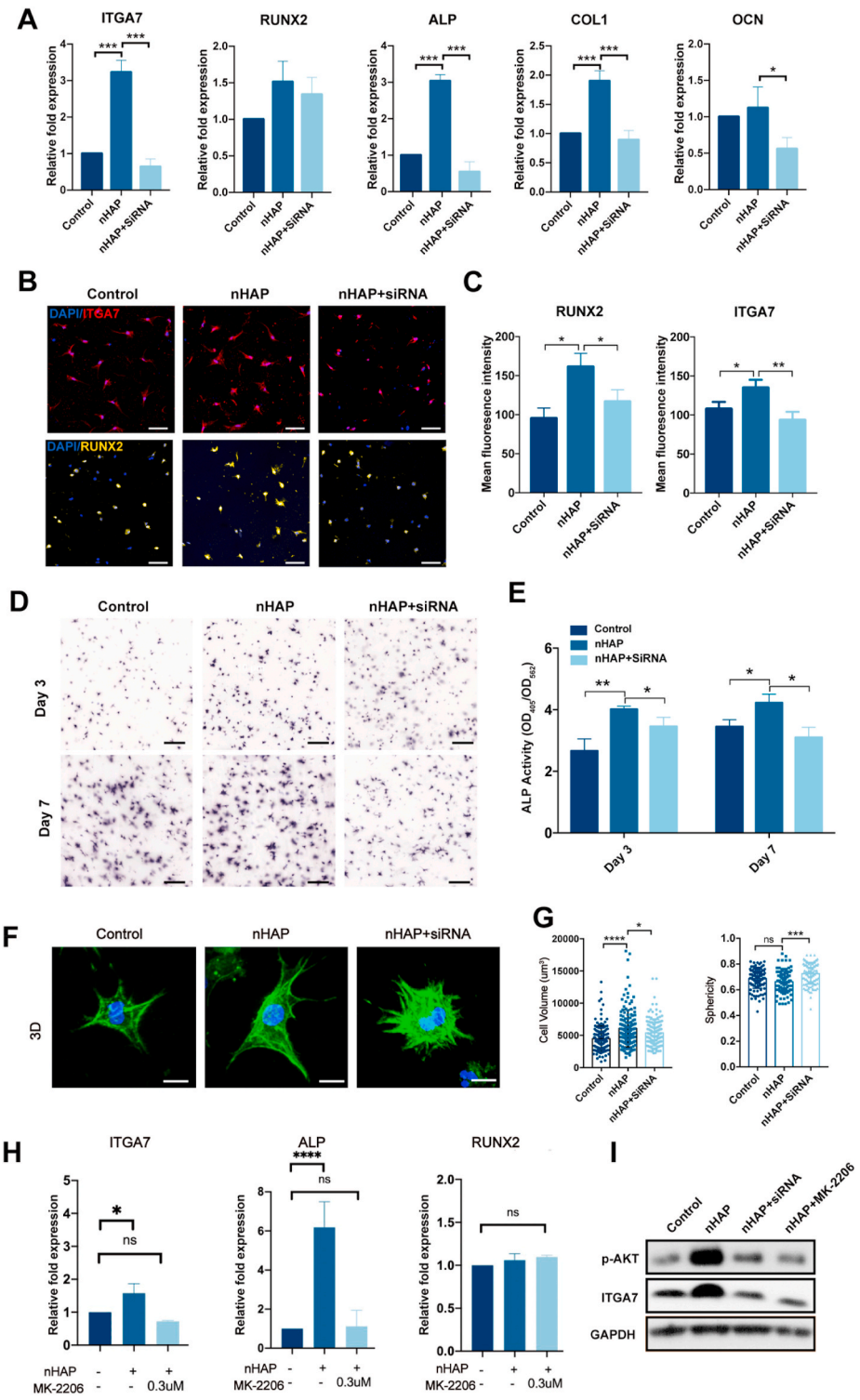


**Fig. 5.** ITGA7 regulates cell morphology and osteogenesis in a reciprocal way with PI3K-AKT pathway. (A) Relative gene expression of *ITGA7*, *RUNX2*, *ALP*, *COL1*, *OCN* in 3D groups for 3 days. (B) Immunofluorescence staining of RUNX2 and ITGA7 and corresponding quantifications (C) of hBMSCs in 3D groups for 3 days. Scale bar = 50 μm. (D) ALP staining D) and corresponding quantification (E) in 3D-nHAP groups. Scale bar = 200 μm. (F) Representative confocal images of single cell and corresponding quantification (G) in 3D groups. Scale bar = 10 μm (n = 3, more than 100 single cells were counted). (H) Relative mRNA expression level of ITGA7, RUNX2 and ALP after inhibiting the PI3K-AKT signaling pathway. (I) Protein expression level of ITGA7 and p-AKT with ITGA7 knockdown or the inhibitor of PI3K-AKT pathway determined by Western blot. *p < 0.05, **p < 0.01, ***p < 0.001, ****p < 0.0001.

different microenvironments influence the osteogenic differentiation of hBMSCs, we designed and examined three experimental groups as well as their corresponding control groups. This not only enables us to compare each nHAP group with the corresponding control group in terms of the applied form, but also makes possible the comparison between the different applied forms of nanoparticles. Our results demonstrated that hBMSCs exhibited enhanced osteogenic ability with marked volume expansion in the 3D-nHAP group and exhibited a less-than-optimal tendency in Coating-nHAP, whereas inhibited osteogenesis with decreased spreading areas were observed in Free-nHAP microenvironment. ITGA7 was identified to play an important role during the early stage of osteogenesis via the PI3K-AKT signaling pathway. *In vivo* experiments further confirmed the differential effects of free and fixed nHAP in the regulation of osteogenesis and ITGA7 expression of hBMSCs.

Firstly, we found that osteogenesis was significantly promoted with fixed state of nHAP in 3D. And in coating microenvironment, it was promoted only to a small degree, whereas it was inhibited with free state of nHAP. The osteogenic effects of free hydroxyapatite remain controversial. Free HAP has been reported to induce proinflammatory and

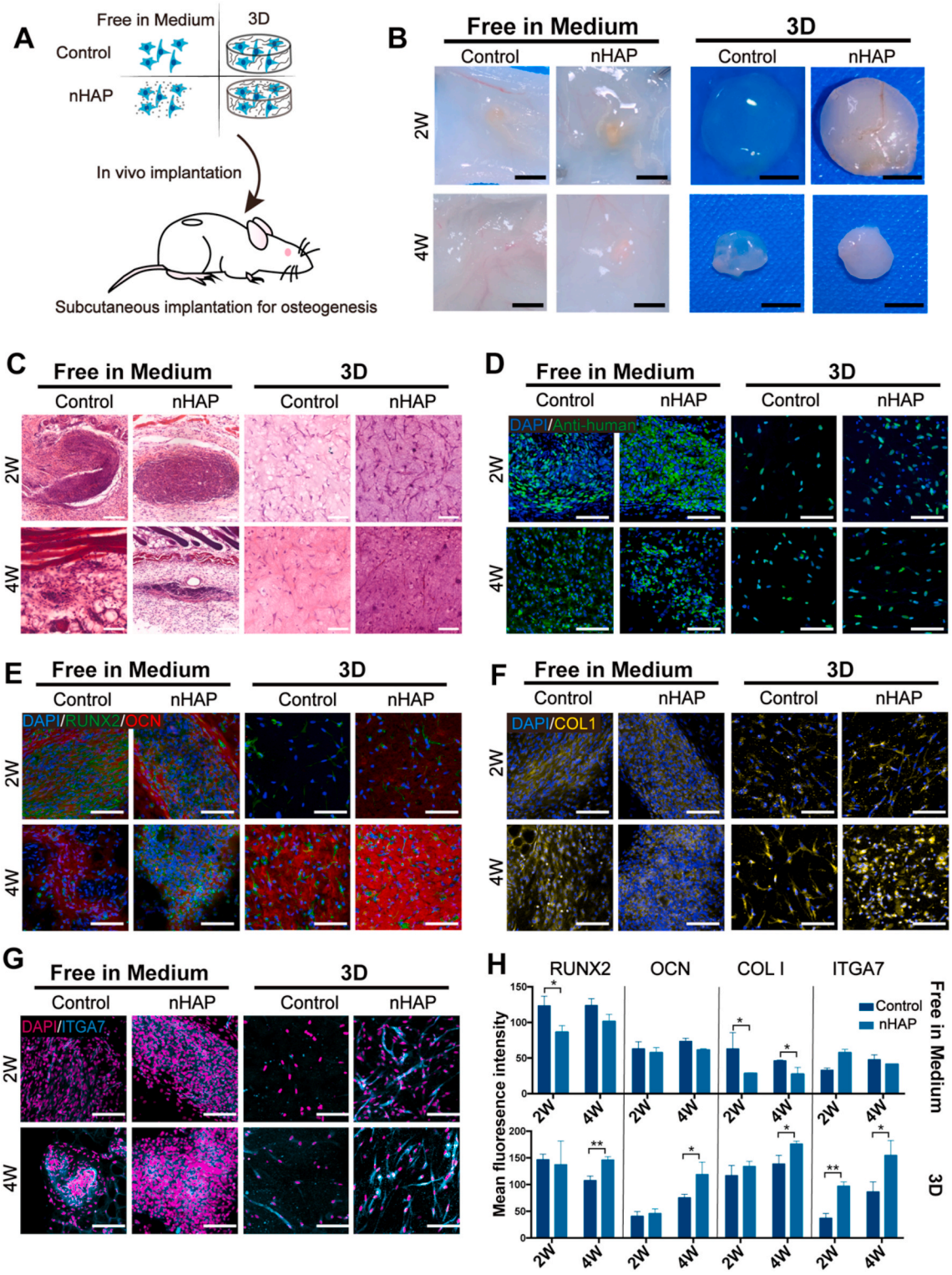


**Fig. 6.** 3D-nHAP microenvironment promotes the expression of ITGA7 and osteogenesis, whereas not Free-nHAP microenvironment *in vivo*. (A) Illustration of the subcutaneous implantation of Free and 3D groups. (B) Gross images after 2-week and 4-week implantation. Scale bar = 2 mm for Free groups. Scale bar = 4 mm for 3D groups. (C) H&E staining for the grafts after 2 and 4 weeks. (D) Immunofluorescence staining of human-specific lamin for hBMSCs in the grafts after 2 and 4 weeks. Scale bar = 100 μm. (E) Immunofluorescence staining of RUNX2 and OCN of the grafts after 2 and 4 weeks. Scale bar = 100 μm. (F) and (G) Immunofluorescence staining of COL1 (F) and ITGA7 (G) of the grafts after 2 and 4 weeks. Scale bar = 100 μm. (H) Qualification of immunofluorescence staining of RUNX2, OCN, COL1 and ITGA7.

osteoclastogenic effects on human mononuclear cells and negatively regulate the proliferation of osteoblasts *in vitro* [25]. Other studies reported that free HAP did not support bone healing and growth *in vivo* [26]. In contrast, Yao et al. injected a free-flowing calcium phosphate material into the mice osteoporotic tibia in order to remineralize the collagen fibrils, and revealed that the repaired bones exhibit satisfactory mechanical performance comparable with normal bones [3]. Taken together, it can be inferred that the direct assembly of freely-suspended HAP and cells is not an optimal way, but the freely-suspended HAP could be exploited by mineralizing other materials for tissue engineering. With regards to the Coating applied form, Wu et al. found that nHAP coated materials properties affected osteogenesis and angiogenesis, and that its nanoscale topography altered integrin binding specificity [27]. The underlying mechanism of these observed changes might be consistent with our data of RNA-seq [27]. In addition, compared with the Free in Medium groups, these results suggested that cells in the Coating groups enhanced osteogenic differentiation when the microenvironment of nHAP was changed from free to fixed under the same conventional culture condition. 3D-nHAP microenvironment has been widely applied for bone tissue engineering via be incorporated into composite biomaterials [23]. Previous studies had reported that the intrafibrillar deposition of nHAP on collagen can promote formation of vascularized bone-like tissue construction and promote the osteogenesis of BMSCs and bone repair, respectively [28,29]. Although nHAP was not applied to mimic the complexity of bone's nanoscale calcification and mineral formation, the low concentration of nHAP in GelMA still exhibited a pronounced effect on osteogenesis. Collectively, these findings imply the utility of cell-laden 3D-nHAP hydrogels in tissue engineering applications, which may provide an superior alternative for closely mimicking the 3D structure of the cell-rich bone matrix more closely.

Furthermore, we elucidated that ITGA7 played an important role at the early stage of osteogenesis through the PI3K-AKT signaling pathway. Previous studies on ITGA7 revealed its association with tumor invasion and metastasis [30,31]. ITGA7 is also known to be specific for skeletal muscle and is expressed mainly during myogenic differentiation [32]. However, little is known about the role of ITGA7 in osteogenesis. A study concerning osteoporosis found that ITGA7 was significantly down-regulated after ovariectomy operations compared with the sham group [33]. Our study has, for the first time, correlated osteogenesis with ITGA7 expression and demonstrated that increasing ITGA7 expression promoted osteogenesis in the 3D-nHAP and Coating-nHAP groups, while reducing ITGA7 expression inhibited osteogenesis in the Free-nHAP group. Interestingly, cells cultured in a 3D microenvironment displayed the lowest level of ITGA7 expression, as compared to that in Free in Medium and Coating groups, which is likely due to their inherent culturing systems. Despite the lowest expression level of ITGA7 observed in cells cultured in a 3D microenvironment, osteogenic differentiation was markedly promoted with such nHAP applied form via increased expression of ITGA7. The AKT pathway has been related to the osteogenesis of BMSCs [22]. Our study has also revealed that the AKT pathway mediated 3D-nHAP microenvironment-induced osteogenesis, and the pathway is regulated by ITGA7 under this condition. Collectively, we to some extent fill the gap about the mechanism of 3D-nHAP microenvironment-induced osteogenesis.

In addition, we observed that the different applied form of nHAP can induce changes to cell morphology that correlates with osteogenic differentiation. Previous studies have demonstrated that the regulatory effects of physical and mechanical properties of the cellular microenvironment upon cell shape and cell fate [34]. McBeath and his colleagues have found that cell shape regulates the commitment of hMSCs to the adipogenic or osteogenic fate within 2D culture [35]. In recent studies on cell volume, both scenarios (reduced cell volume and increased cell volume) have been reported to promote osteogenesis [21,36]. However, still little is known about the correlation between cell morphology and differentiation processes when cells are exposed to different nHAP applied forms. Cell volume expanded when cells were encapsulated in nHAP nanocomposite hydrogels, which increased the roughness of hydrogels that might facilitate cell adhesion and migration. However, in the Free in Medium group, nHAP were absorbed on cell membrane, diminishing the amount of filipodia, which led to reduced cell spreading areas and slender cell shape. Ma et al. found that the exposure of gold nanoparticles induced a more elongated, stretched cell shape and reduced the cellular cross-sectional area [37], which is consistent with our results. In the Coating-nHAP group, the changes in cell morphology were subtle in comparison with those of the Free in Medium groups due to the lack of significant change in circularity in this group. The lack of significant differences, combined with the results of 3D groups, also suggested that the fixed state of nHAP have a totally different outcome in terms of cell morphology.

However, it is important to note that this study has several potential limitations. Despite the same nHAP concentration utilized in different applied forms, the number of nanoparticles directl contacted with cells were different under real experimental conditions. Hence, the Coating groups have fewer differences in cell morphology partly because of the smaller amount of nHAP used compared with that of the Free in Medium and 3D groups. However, the results at the gene expression level suggested that nHAP can promote osteogenesis when fixed on a surface. Another limitation is the failure to mimic the bone structure, a sophisticated composite structure with different hierarchical levels. Finally, intrafibrillar mineral should be better mimicked to investigate corresponding mechanism as an important way for the application of nHAP, and this model should be compared with others.

In conclusion, we compared how cells behaved and differentiated in free and fixed state of nHAP (e.g., Free in Medium, Coating and 3D), and demonstrated that free and fixed state of nHAP can differentially alter cell morphology and osteogenic differentiation. Furthermore, our research demonstrated the key role of ITGA7 in osteogenic differentiation, which could potentially be a new molecular target for bone tissue engineering and therapy, as well as provided important cues on how nanoparticles should be used in biomedical applications.

## 4. Methods

### 4.1. Design of experimental groups

In order to systematically investigate the effects of the different applied forms of nHAP, the experiments were conducted with three applied nHAP forms in six groups (Fig. 1A). Each applied form was paired with its own control group and experimental group to eliminate the impacts of other factors. In the Free in medium group, pure hBMSCs were cultured on a dish as a control group (Free-con), while hBMSCs treated with nHAP in culture medium were assigned as the experimental group (Free-nHAP). In the other two applied forms, nHAP was added into GelMA to obtain nanocomposite hydrogels (GelMA-nHAP). In the Coating groups, GelMA coating was assigned as a control group (Coating-con), while GelMA-nHAP coating was assigned as an experimental group (Coating-nHAP). As for 3D culture, hBMSCs-laden GelMA group was assigned as a control group (3D-con), while hBMSCs-laden GelMA-nHAP group was assigned as an experimental group (3D-nHAP).

### 4.2. GelMA preparation

Porcine skin gelatin (Sigma) was dissolved into phosphate buffered saline (PBS) at 10% (w/v) and stirred at 60 °C until fully dissolved. Methacrylic anhydride (MA) was slowly added (0.5 mL/min) into the gelatin solution to reach the target volume under stirred conditions at 50 °C, which was then allowed to react for 4 h. The mixture was then dialyzed against distilled water by using a 12–14 kDa cutoff dialysis tubing at 40 °C to remove salts and MA. After 1 week, the solution was lyophilized for another 1 week and stored at −80 °C for further use.

### 4.3. Cell viability and proliferation

hBMSCs were cultured with growth medium containing low-glucose DMEM (L-DEME, Gibco) supplemented with 10% fetal bovine serum (FBS, Gibco) and 1% penicillin/streptomycin (P/S, Gibco). Cell viability was assayed by Live/Dead assay (DOJINDO) after 1, 3, and 7 days. Briefly, Cellstain-PI (1 μL/mL in PBS) and Calcein-AM (1 μL/mL in PBS) were added and incubated for 30 min at 37 °C for staining dead cells and live cells, respectively. The samples were then washed with PBS for three times to remove the remaining stains. The stained samples were then imaged and analyzed using ImageJ software (National Institutes of Health, USA). Cell viability (%) was calculated by dividing the number of live cells by the number of total cells.

### 4.4. Preparation of Coaing-nHAP and 3D-nHAP

In the 3D-nHAP group, cells, nHAP and GelMA solution were mixed prior to cross-linking to achieve a final cell concentration of $5 \times 10^6$ cells/mL, final 10 wt% GelMA solution and final 167 μg/ml nHAP concentration. Then, the mixture was dripped onto cell culture dishes followed by 20 s of UV irradiation to form hydrogel. In the Coating-nHAP group, nHAP and GelMA solution were mixed prior to cross-linking to achieve a final 167 μg/ml nHAP concentration and final 10 wt% GelMA solution. Then, the mixture was added onto the culture plates. After being spread evenly on the plates, then most of the liquid was sucked out, leaving only a thin layer for UV-induced crosslinking. Finally, hBMSCs were seeded onto the thin layer for different experiments. Corresponding controls did not contain nHAP while other components were the same as experimental groups.

### 4.5. Scanning electron microscopy

In the Free and Coating groups, samples were fixed overnight using 2.5% (w/v) glutaraldehyde at 4 °C, followed by three times of PBS rinses. After 1h incubation in 1% (w/v) osmium tetroxide, the samples were dehydrated using an ethanol gradient series (30%, 50%, 70%, 90%, 95% and 100%) and dried in a Critical Point Drier. Scanning electron microscope was used to characterize the cell morphology on surfaces. For 3D hydrogel samples, they were fixed overnight at 4 °C in 2.5% (w/v) glutaraldehyde followed by three times of PBS rinses. The fixed samples were pre-frozen and lyophilized for SEM.

### 4.6. ALP staining and activity quantification

Cells were cultured for 3 days and 7 days in osteogenic induction medium. The osteogenic induction medium contained growth medium with 50 μg/ml L-ascorbic acid (Sigma) and 10 mM β-glycerophosphate (Sigma) and 0.1 μM dexamethasone (Sigma). A commercially available ALP staining kit (Beyotime) was used to stain ALP according to manufacturer's instructions. ALP quantification kit (Beyotime) and protein quantification kit (Beyotime) were used to measure the activity of ALP and total protein according to manufacturer's instructions [38].

### 4.7. Immunofluorescence staining

To visualize the expression of osteogenic markers, all samples for the experiments were cultured in osteogenic induction medium for 3 days and 7 days. and then fixed with 4% (w/v) paraformaldehyde (PFA) for 20 min. After fixation, cells were washed in PBS and permeabilized in 0.1% (w/v) Triton X-100 for 10 min. Then 1% (w/v) bovine serum albumin (BSA) was used for 1h at room temperature. The specific primary antibody was diluted in 1% (w/v) BSA and the samples were incubated overnight at 4 °C. This was then followed by incubation with secondary antibody diluted in PBS for 2h and DAPI (1:10000, Beyotime) for 10 min. There were several additional steps for 3D groups samples. After fixation, dehydration was conducted with 10% (w/v) and 30% (w/v) sucrose solution until the sample sank to the bottom, followed by embedment with OCT for frozen sectioning, with each slice being 50 μm thick. The antibody was listed in supplementary information (Table S1).

### 4.8. Cell morphology analysis

DAPI and phalloidin staining were used for cell morphology assay. 3D groups images stacks were taken using a confocal microscope. Single cells that were not in contact with the others were analyzed. Image stacks with a 2-μm z-axis interval were stacked, and cell volume and sphericity were calculated by Imaris software. For Free and Coating groups, the spreading area and circularity were analyzed using ImageJ software (National Institutes of Health, USA). A circularity and sphericity value of 1.0 indicates a perfect circle or ball, while values approaching 0.0 reflect an increasingly elongated shape.

### 4.9. RNA interfering

After cells reached about 70% confluence, 20 μM siRNA targeting ITGA7 was diluted into Opti-MEM (Gibco), reaching a final concentration of 50 nM. Then Lipofectamine 2000 (ThermoFisher Scientific Inc.) was diluted according to manufacturer's instruction. After 15-min incubation, the diluted siRNA and the diluted Lipofectamine 2000 were further gently mixed followed by another 15-min incubation at room temperature. Then, the siRNA-Lipofectamine 2000 complexes were added into each culture plates. After 4-6 hours, medium was changed. For the 7-day osteogenic induction, cells were transfected with the siRNA twice.

### 4.10. Nanoindentation

The Coating and 3D groups samples were made as described before. Piuma Nanoindenter (Optics11 Life) performed micro scale indentation of hydrogel surface. Nine samples were submerged in PBS at room temperature and the probe was pressed into the samples at a rate of 2 μm/s until 10 μm.

### 4.11. Quantitative real-time PCR

Quantitative real-time PCR (qPCR) was conducted to evaluate the mRNA levels of *RUNX2*, *ALP*, *COL1*, *OCN*, *ITGA7*. At the endpoint of each experiment, the cells were washed twice in PBS and then added with Trizol reagent (Invitrogen-Life Technologies). The primers used for the qPCR analysis in this study are listed in Table S2. qPCR reactions were performed using the TB Green PCR kit (TaKaRa) according to manufacturer's instruction.

### 4.12. Western blot

RIPA lysis buffer containing protease and phosphatase inhibitors (ThermoFisher Scientific Inc.) were used for cell lysis, BCA assay (Beyotime) was used for quantification of the protein concentration. 25 μg total proteins were loaded. And the gels were ran for an hour and half, and the separated proteins were subsequently transferred to PVDF membranes. The membranes were blocked for an hour and then incubated with primary antibodies at 4 °C overnight. After they were incubated with secondary antibodies at room temperature for 1 h, Licor Odyssey imaging system was used for imaging the blots.

### 4.13. Ectopic osteogenesis assay

All the animals were treated according to the guidelines approved by the Zhejiang University Ethics Committee (ZJU20210242). In Free-nHAP and Free-control groups, only hBMSCs or both hBMSCs (1×10^6 cells/ml) and Free-nHAP (167 μg/ml) were directly injected into the subcutaneous area at the back of the nude mice (BALB/c Nude,

6-week old). In 3D-nHAP and 3D-con groups, after the disinfection of the back of the animals with povidone-iodine, we made two longitudinal incisions on both sides of the vertebral column. Then, GelMA hydrogel incorporating only hBMSCs or incorporating both hBMSCs and nHAP was transplanted into the subcutaneous pocket. Finally, the incisions were closed with a degradable suture.

### 4.14. Histological analysis

The subcutaneous pocket, where the hBMSCs, nHAP and hydrogels had been transplanted, were collected at week 2 and week 4 for fixation for 48 hours using PFA. The samples were then embedded by NG-50 (ThermoFisher Scientific Inc.) for frozen section with 50 μm thickness. The sections were stored at −20 °C. For H&E staining, the sections were stained with hematoxylin (Sigma) for 10 min, differentiated by hydrochloric alcohol (Sigma) for 1 s and stained with eosin (Sigma) for 30 s. The slides were imaged by a digital scanner (3DHISTECH). Immunofluorescence staining was similar with those in *vitro*.

### 4.15. RNA-seq

hBMSCs were cultured in Free in Medium, Coating and 3D, and the experimental groups were treated with nHAP exposure (- 167 μg/ml, 7 days). At the end of 7 days of culture, total RNA was extracted (High Pure RNA Isolation, Roche Life Sciences). mRNA purification was performed by oligo(dT)-attached beads. Samples were run in the BGIseq500 platform (BGI-Shenzhen, China).

### 4.16. Statistical analysis

All experiments were analyzed with at least biological triplicates, and the analysis of cell morphology was performed with ≥100 cells. GraphPad Prism 7.0 software (GraphPad Software) was used for statistical comparisons. Multiple group comparisons were performed by one- or two-way ANOVA tests with a Bonferroni post hoc comparison and the comparison of two experimental groups was performed using a two-tailed Student's *t*-test.

## CRediT authorship contribution statement

**Fangyuan Bao:** Conceptualization, Software, Methodology, Investigation, Formal analysis, Writing – original draft, Writing – review & editing. **Junzhi Yi:** Conceptualization, Methodology, Investigation, Formal analysis, Writing – original draft, Writing – review & editing. **Yixiao Liu:** Investigation, Writing – review & editing, Data curation. **Yuliang Zhong:** Investigation, Formal analysis. **Hui Zhang:** Investigation, Formal analysis. **Zhonglin Wu:** Formal analysis. **Boon Chin Heng:** Writing – review & editing. **Ying Wang:** Investigation. **Ziyang Wang:** Visualization. **Hua Liu:** Supervision. **Lizi Xiao:** Writing – review & editing. **Hongwei Ouyang:** Conceptualization, Supervision, Funding acquisition, Project administration. **Jing Zhou:** Conceptualization, Supervision, Project administration, Funding acquisition, Writing – review & editing.

## Declaration of competing interest

The authors hereby declare no relevant conflicts of interests.

## Acknowledgments

This research was supported by the National Key R&D program of China (2018YFC1105100) and the National Natural Science Foundation of China (NSFC grant NO. T2121004 and NO. 31830029). We are grateful for utilization of equipment provided by Core Facilities, Zhejiang University School of Medicine and Analysis Center of Agrobiology and Environmental Sciences, Zhejiang University.

## Appendix A. Supplementary data

Supplementary data to this article can be found online at https://doi.org/10.1016/j.bioactmat.2022.03.016.

## References

[1] A. Salhotra, H.N. Shah, B. Levi, M.T. Longaker, Mechanisms of bone development and repair, Nat. Rev. Mol. Cell Biol. 21 (2020) 696–711, https://doi.org/10.1038/s41580-020-00279-w.
[2] T. Gong, J. Xie, J. Liao, T. Zhang, S. Lin, Y. Lin, Nanomaterials and bone regeneration, Bone Res. 3 (2015) 15029, https://doi.org/10.1038/boneres.2015.29.
[3] S. Yao, X. Lin, Y. Xu, Y. Chen, P. Qiu, C. Shao, B. Jin, Z. Mu, N.A.J.M. Sommerdijk, R. Tang, Osteoporotic bone recovery by a highly bone-inductive calcium phosphate polymer-induced liquid-precursor, Adv. Sci. (2019) 1900683, https://doi.org/10.1002/advs.201900683.
[4] L. Bai, Z. Du, J. Du, W. Yao, J. Zhang, Z. Weng, S. Liu, Y. Zhao, Y. Liu, X. Zhang, X. Huang, X. Yao, R. Crawford, R. Hang, D. Huang, B. Tang, Y. Xiao, A multifaceted coating on titanium dictates osteoimmunomodulation and osteo/angio-genesis towards ameliorative osseointegration, Biomaterials 162 (2018) 154–169, https://doi.org/10.1016/j.biomaterials.2018.02.010.
[6] O.R. Mahon, D.C. Browe, T. Gonzalez-Fernandez, P. Pitacco, I.T. Whelan, S. Von Euw, C. Hobbs, V. Nicolosi, K.T. Cunningham, K.H.G. Mills, D.J. Kelly, A. Dunne, Nano-particle mediated M2 macrophage polarization enhances bone formation and MSC osteogenesis in an IL-10 dependent manner, Biomaterials 239 (2020) 119833, https://doi.org/10.1016/j.biomaterials.2020.119833.
[7] Y. Yang, T. Xu, Q. Zhang, Y. Piao, H.P. Bei, X. Zhao, Biomimetic, stiff, and adhesive periosteum with osteogenic–angiogenic coupling effect for bone regeneration, Small 17 (2021) 2006598, https://doi.org/10.1002/smll.202006598.
[8] A. Pirosa, R. Gottardi, P.G. Alexander, D. Puppi, F. Chiellini, R.S. Tuan, An in vitro chondro-osteo-vascular triphasic model of the osteochondral complex, Biomaterials 272 (2021), https://doi.org/10.1016/j.biomaterials.2021.120773, 120773.
[9] M. Farokhi, F. Mottaghitalab, S. Samani, M.A. Shokrgozar, S.C. Kundu, R.L. Reis, Y. Fatahi, D.L. Kaplan, Silk fibroin/hydroxyapatite composites for bone tissue engineering, Biotechnol. Adv. 36 (2018) 68–91, https://doi.org/10.1016/j.biotechadv.2017.10.001.
[10] S.H. Lim, H.-Q. Mao, Electrospun scaffolds for stem cell engineering, Adv. Drug Deliv. Rev. 61 (2009) 1084–1096, https://doi.org/10.1016/j.addr.2009.07.011.
[11] H.-S. Kim, J.-H. Lee, N. Mandakhbayar, G.-Z. Jin, S.-J. Kim, J.-Y. Yoon, S.B. Jo, J.-H. Park, R.K. Singh, J.-H. Jang, U.S. Shin, J.C. Knowles, H.-W. Kim, Therapeutic tissue regenerative nanohybrids self-assembled from bioactive inorganic core/chitosan shell nanounits, Biomaterials 274 (2021) 120857, https://doi.org/10.1016/j.biomaterials.2021.120857.
[12] Z. Hamidouche, O. Fromigue, J. Ringe, S. Srouji, E. Livne, P.J. Marie, Priming integrin alpha5 promotes human mesenchymal stromal cell osteoblast differentiation and osteogenesis. Proc. Natl. Acad. Sci. U.S.A. 2009 Nov 3;106(44): 18587-91. doi: 10.1073/pnas.0812334106.
[13] B. Shen, K. Vardy, P. Hughes, A. Tasdogan, Z. Zhao, R. Yue, G.M. Crane, S. J. Morrison, Integrin alpha11 is an Osteolectin receptor and is required for the maintenance of adult skeletal bone mass, eLife 8 (2019), e42274, https://doi.org/10.7554/eLife.42274.
[14] K. Yue, G. Trujillo-de Santiago, M.M. Alvarez, A. Tamayol, N. Annabi, A. Khademhosseini, Synthesis, properties, and biomedical applications of gelatin methacryloyl (GelMA) hydrogels, Biomaterials 73 (2015) 254–271, https://doi.org/10.1016/j.biomaterials.2015.08.045.
[15] C. Shao, R. Zhao, S. Jiang, S. Yao, Z. Wu, B. Jin, Y. Yang, H. Pan, R. Tang, Citrate improves collagen mineralization via interface wetting: a physicochemical understanding of biomineralization control, Adv. Mater. 30 (2018) 1704876, https://doi.org/10.1002/adma.201704876.
[16] W.L. Suchanek, K. Byrappa, P. Shuk, R.E. Riman, V.F. Janas, K.S. TenHuisen, Preparation of magnesium-substituted hydroxyapatite powders by the mechanochemical–hydrothermal method, Biomaterials 25 (2004) 4647–4657, https://doi.org/10.1016/j.biomaterials.2003.12.008.
[17] F. Wan, H. Ping, W. Wang, Z. Zou, H. Xie, B.-L. Su, D. Liu, Z. Fu, Hydroxyapatite-reinforced alginate fibers with bioinspired dually aligned architectures, Carbohydr. Polym. 267 (2021) 118167, https://doi.org/10.1016/j.carbpol.2021.118167.
[19] P.K. Mattila, P. Lappalainen, Filopodia: molecular architecture and cellular functions, Nat. Rev. Mol. Cell Biol. 9 (2008) 446–454, https://doi.org/10.1038/nrm2406.
[20] J.K. Carrow, K.A. Singh, M.K. Jaiswal, A. Ramirez, G. Lokhande, A.T. Yeh, T. R. Sarkar, I. Singh, A.K. Gaharwar, Photothermal modulation of human stem cells using light-responsive 2D nanomaterials, Proc. Natl. Acad. Sci. 117 (2020) 13329–13338, https://doi.org/10.1073/pnas.1914345117.
[21] H. Lee, R. Stowers, O. Chaudhuri, Volume expansion and TRPV4 activation regulate stem cell fate in three-dimensional microenvironments, Nat. Commun. 10 (2019) 529, https://doi.org/10.1038/s41467-019-08465-x.
[22] C. Yang, X. Liu, K. Zhao, Y. Zhu, B. Hu, Y. Zhou, M. Wang, Y. Wu, C. Zhang, J. Xu, Y. Ning, D. Zou, miRNA-21 promotes osteogenesis via the PTEN/PI3K/Akt/HIF-1α pathway and enhances bone regeneration in critical size defects, Stem Cell Res. Ther. 10 (2019) 65, https://doi.org/10.1186/s13287-019-1168-2.
[23] G. Thrivikraman, A. Athirasala, R. Gordon, L. Zhang, R. Bergan, D.R. Keene, J. M. Jones, H. Xie, Z. Chen, J. Tao, B. Wingender, L. Gower, J.L. Ferracane, L.

E. Bertassoni, Rapid fabrication of vascularized and innervated cell-laden bone models with biomimetic intrafibrillar collagen mineralization, Nat. Commun. 10 (2019) 3520, https://doi.org/10.1038/s41467-019-11455-8.
[24] F. Wu, W. Chen, B. Gillis, C. Fischbach, L.A. Estroff, D. Gourdon, Protein-crystal interface mediates cell adhesion and proangiogenic secretion, Biomaterials 116 (2017) 174–185, https://doi.org/10.1016/j.biomaterials.2016.11.043.
[25] T. Lange, A.F. Schilling, F. Peters, F. Haag, M.M. Morlock, J.M. Rueger, M. Amling, Proinflammatory and osteoclastogenic effects of beta-tricalciumphosphate and hydroxyapatite particles on human mononuclear cells in vitro, Biomaterials 30 (2009) 5312–5318, https://doi.org/10.1016/j.biomaterials.2009.06.023.
[26] O. Rahbek, S. Kold, K. Bendix, S. Overgaard, K. Soballe, No effect of hydroxyapatite particles in phagocytosable sizes on implant fixation: an experimental study in dogs, J. Biomed. Mater. Res. A. 73A (2005) 150–157, https://doi.org/10.1002/jbm.a.30245.
[27] F. Wu, W. Chen, B. Gillis, C. Fischbach, L.A. Estroff, D. Gourdon, Protein-crystal interface mediates cell adhesion and proangiogenic secretion, Biomaterials 116 (2017) 174–185, https://doi.org/10.1016/j.biomaterials.2016.11.043.
[28] G. Thrivikraman, A. Athirasala, R. Gordon, L. Zhang, R. Bergan, D.R. Keene, J. M. Jones, H. Xie, Z. Chen, J. Tao, B. Wingender, L. Gower, J.L. Ferracane, L. E. Bertassoni, Rapid fabrication of vascularized and innervated cell-laden bone models with biomimetic intrafibrillar collagen mineralization, Nat. Commun. 10 (2019) 3520, https://doi.org/10.1038/s41467-019-11455-8.
[29] J. Li, J.-F. Yan, Q.-Q. Wan, M.-J. Shen, Y.-X. Ma, J.-T. Gu, P. Gao, X.-Y. Tang, F. Yu, J.-H. Chen, F.R. Tay, K. Jiao, L.-N. Niu, Matrix stiffening by self-mineralizable guided bone regeneration, Acta Biomater. 125 (2021) 112–125, https://doi.org/10.1016/j.actbio.2021.02.012.
[30] X.-Y. Ming, L. Fu, L.-Y. Zhang, Y.-R. Qin, T.-T. Cao, K.W. Chan, S. Ma, D. Xie, X.-Y. Guan, Integrin α7 is a functional cancer stem cell surface marker in oesophageal squamous cell carcinoma, Nat. Commun. 7 (2016) 13568, https://doi.org/10.1038/ncomms13568.
[31] T.L. Haas, M.R. Sciuto, L. Brunetto, C. Valvo, M. Signore, M.E. Fiori, S. di Martino, S. Giannetti, L. Morgante, A. Boe, M. Patrizii, U. Warnken, M. Schnölzer, A. Ciolfi, C. Di Stefano, M. Biffoni, L. Ricci-Vitiani, R. Pallini, R. De Maria, Integrin α7 is a functional marker and potential therapeutic target in glioblastoma, Cell Stem Cell 21 (2017) 35–50, https://doi.org/10.1016/j.stem.2017.04.009, e9.
[32] K.N. Heller, C.L. Montgomery, P.M. Janssen, K.R. Clark, J.R. Mendell, L.R. Rodino-Klapac, AAV-mediated overexpression of human α7 integrin leads to histological and functional improvement in dystrophic mice, Mol. Ther. 21 (2013) 520–525, https://doi.org/10.1038/mt.2012.281.
[33] T. Huang, Z. Yu, Q. Yu, Y. Wang, Z. Jiang, H. Wang, G. Yang, Inhibition of osteogenic and adipogenic potential in bone marrow-derived mesenchymal stem cells under osteoporosis, Biochem. Biophys. Res. Commun. 525 (2020) 902–908, https://doi.org/10.1016/j.bbrc.2020.03.035.
[34] G. Halder, S. Dupont, S. Piccolo, Transduction of mechanical and cytoskeletal cues by YAP and TAZ, Nat. Rev. Mol. Cell Biol. 13 (2012) 591–600, https://doi.org/10.1038/nrm3416.
[35] R. McBeath, D.M. Pirone, C.M. Nelson, K. Bhadriraju, C.S. Chen, Cell shape, cytoskeletal tension, and RhoA regulate stem cell lineage commitment, Dev. Cell 6 (2004) 483–495, https://doi.org/10.1016/S1534-5807(04)00075-9.
[36] M. Guo, A.F. Pegoraro, A. Mao, E.H. Zhou, P.R. Arany, Y. Han, D.T. Burnette, M. H. Jensen, K.E. Kasza, J.R. Moore, F.C. Mackintosh, J.J. Fredberg, D.J. Mooney, J. Lippincott-Schwartz, D.A. Weitz, Cell volume change through water efflux impacts cell stiffness and stem cell fate, Proc. Natl. Acad. Sci. 114 (2017) E8618–E8627, https://doi.org/10.1073/pnas.1705179114.
[37] X. Ma, R. Hartmann, D. Jimenez de Aberasturi, F. Yang, S.J.H. Soenen, B. B. Manshian, J. Franz, D. Valdeperez, B. Pelaz, N. Feliu, N. Hampp, C. Riethmüller, H. Vieker, N. Frese, A. Gölzhäuser, M. Simonich, R.L. Tanguay, X.-J. Liang, W. J. Parak, Colloidal gold nanoparticles induce changes in cellular and subcellular morphology, ACS Nano 11 (2017) 7807–7820, https://doi.org/10.1021/acsnano.7b01760.
[38] Y. Liu, J. Fang, Q. Zhang, X. Zhang, Y. Cao, W. Chen, Z. Shao, S. Yang, D. Wu, M. Hung, Y. Zhang, W. Tong, H. Tian, Wnt10b-overexpressing umbilical cord mesenchymal stem cells promote critical size rat calvarial defect healing by enhanced osteogenesis and VEGF-mediated angiogenesis, J. Orthop. Transl. 23 (2020) 29–37, https://doi.org/10.1016/j.jot.2020.02.009.
[39] J. Radhakrishnan, A. Manigandan, P. Chinnaswamy, A. Subramanian, S. Sethuraman, Gradient nano-engineered in situ forming composite hydrogel for osteochondral regeneration, Biomaterials 162 (2018) 82–98, https://doi.org/10.1016/j.biomaterials.2018.01.056.
[40] J. Zhang, J. Jia, J.P. Kim, H. Shen, F. Yang, Q. Zhang, M. Xu, W. Bi, X. Wang, J. Yang, D. Wu, Ionic colloidal molding as a biomimetic scaffolding strategy for uniform bone tissue regeneration, Adv. Mater. 29 (2017) 1605546, https://doi.org/10.1002/adma.201605546.